**SIRM 2015 – 11th International Conference on Vibrations in Rotating Machines,
Magdeburg, Deutschland, 23. – 25. February 2015**

Influence of axial grooves in full-floating-ring bearings on the nonlinear oscillations of turbocharger rotors

Gerrit Nowald [1], Aydin Boyaci [1], Robert Schmoll [2], Panagiotis Koutsovasilis [3], Nicolas Driot [3], Bernhard Schweizer [1]

[1] Fachgebiet Strukturdynamik, Technische Universität Darmstadt, 64287, Darmstadt, Germany, nowald@sds.tu-darmstadt.de
[2] Institut für Mechanik, Universität Kassel, 34125, Kassel, Germany
[3] BorgWarner Turbo Systems Engineering GmbH, 67292, Kirchheimbolanden, Germany

Abstract

Turbochargers represent rotor systems with high rotation speed, low weight and low static load. They are usually supported in floating-ring bearings and subject to different nonlinear phenomena. Especially subsynchronous oscillations cause undesired acoustic effects in automotive applications. Numerical simulations are an economic and fast way to investigate the influence of different bearing parameters and geometries on the nonlinear oscillation behavior. Here, a coupled model is used in order to analyze the effect of axial grooves on the subsynchronous oscillations. The turbocharger rotor is modeled as a flexible multibody model. The hydrodynamic bearing forces and torques are calculated with a finite-element model. The pressure and sheer stress distributions in the oil films change due to the modified boundary conditions introduced by the grooves. Furthermore, the rotation of the rings and thus the position of the grooves has to be taken into account. Results of run-up simulations for a turbocharger rotor in full-floating-ring bearings are presented for both the plain cylindrical bearing and the bearing with axial grooves.

1 Introduction

High-speed automotive turbocharger rotors are often supported in floating-ring bearings due to their good damping behavior, their reduced friction and their low costs. These rotor-bearing systems show various nonlinear effects such as self-excited vibrations, oil whirl/whip, subharmonics, superharmonics, combination frequencies and jump phenomena [15, 18]. Subsynchronous oscillations often have amplitudes exceeding those of the synchronous imbalance oscillation and frequently cause acoustic problems. In addition, a synchronization of the oil whirl/whip of the inner and the outer oil film can occur in full-floating-ring bearings, which may result in the destruction of the turbocharger [17].

Turbocharger systems have been investigated in recent literature, both experimentally and numerically. The nonlinear effects have been analyzed by different authors based on experimental results and by means of run-up simulations with a dynamic model of the rotor/bearing system, see for instance refs. [13, 14, 16, 20]. Numerical simulations provide a fast and cost-effective way to analyze the effects of different parameters on the oscillation behavior during the design process. Nevertheless, experiments are essential in order to verify numerical models and to gain further insight into the behavior of the dynamical system.

Kirk [7] has performed a large number of experiments with turbocharger rotors in different full-floating-ring geometries with the aim to reduce subsynchronous oscillations. An important parameter for the dynamical bifurcation behavior of turbocharger rotors is the ring speed. Köhl and Kreschel [9] have carried out measurements of the rotation speed of floating-rings.

Recently, different authors have accomplished run-up simulations based on nonlinear turbocharger models. For example, Daniel et al. [4] performed a sensitivity analysis with design methods, using a multibody model with a Timoshenko beam. Nitzschke et al. [13] have investigated the influence of a misaligned bearing and the effect of oil feed holes by means of a numerical run-up simulation. Tomm et al. [20] have investigated different bifurcation scenarios during a rotor run-up with a flexible multibody model and compared simulations with measurements. Busch and Schweizer [3] developed an interface for the coupling of a commercial multibody software and a finite-element software and performed run-up simulations of a turbocharger in full-floating-ring bearings.

It should finally be stressed that the numerical investigations of turbochargers in literature mainly have been carried out considering cylindrical bearings with plain surfaces. The bearings of the floating-rings usually contain grooves to maintain the oil supply. It was also shown in [7] that floating-rings with axial grooves can lower the amplitude of subsynchronous oscillations.

Classical hydrodynamic bearings with complicated geometries have been comprehensively discussed in literature, see for example refs. [11, 12]. It has been shown that multilobe bearings can rise the onset frequency of instability, see e.g. [5, 10]. Yet, only little literature concerning axial grooves in cylindrical bearings can be found. Theoretical predicted stability maps for a rigid rotor in hydrodynamic bearings with axial grooves for different load orientations are shown in [5]. These stability maps have been compared to experimental results in [6]. Nevertheless, most of the studies treat single oil-film bearings under stationary conditions. In literature, mostly simple rotor models – such as rigid rotors or Jeffcott rotors – have been used to study the effects of non-cylindrical bearing geometries on the stability of the rotor system.

Here, the influence of axial grooves in full-floating-ring bearings on the subsynchronous oscillations of turbocharger rotors is investigated. The numerical model used for the studies is described in the next section. Results of run-up simulations with plain cylindrical floating-rings and floating-rings with axial grooves are shown in section 3.

2 Numerical Model of the Turbocharger

In this paper, a semi-implicit coupling approach is used for the numerical simulation of the rotor/bearing system, see ref. [3]. The decomposition of the system in a rotor model and a bearing model is achieved with a force/displacement coupling approach.

The equations of motion for the turbocharger rotor consist of a set of nonlinear differential-algebraic equations (DAE). Here, the commercial multibody system (MBS) software *Adams* from MSC Software has been used for the numerical integration of the DAE system. The rotor model is described in detail in the next section. The bearing forces and torques are calculated with a finite-element model (FEM). Therefore, almost arbitrary geometries and boundary conditions can be realized and a high physical accuracy can be achieved. The commercial software *COMSOL Multiphysics* has been used. The bearing model is illustrated in section 2.2. The coupling procedure between the MBS and FEM software is explained in section 2.3.

2.1 Rotor Model

Figure 1 shows a turbocharger rotor with full-floating-ring bearings. The rotor consists of a flexible shaft and two rigid bodies, namely the compressor wheel and the the turbine wheel. It is assumed that imbalances are located at the compressor and turbine wheel. The shaft is represented by a modally reduced finite-element structure. The turbocharger is subject to gravity.

The floating-rings are modeled as rigid bodies and prevented from tilting with constraints. Axial thrust is not considered in this study. The floating-rings feature three axial grooves in their inner surfaces. The outer surfaces of the floating-rings are assumed plain. Journal bearing forces and torques act on the shaft and the floating-rings,

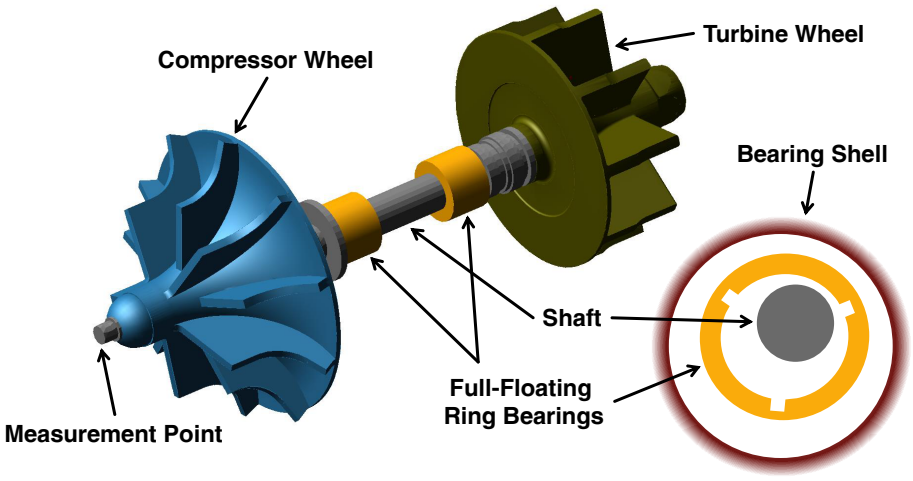

Figure 1: Turbocharger rotor with full-floating-ring bearings.

corresponding to each oil film. In the model, four oil films exist altogether. The turbocharger is kinematically driven by means of a pre-defined rotation speed of the turbine. When the shaft is rotating, the sheer torque in the inner oil film drives the floating-rings, which can otherwise rotate freely. A decelerating sheer torque in the outer oil film develops when the floating-rings begin to rotate. The temperature of the oil is considered by means of the effects on the dynamic viscosity η and on the relative bearing clearances ψ in the inner and the outer oil film. The temperatures are considered constant during a simulation.

2.2 Bearing Model

The geometry of a cylindrical bearing with three axial grooves is shown in Figure 2. The bearing shell has the width B and the radius R. The nominal gap size is denoted by c, the film thickness is cH with the dimensionless gap function $H(\Theta) = 1 + \varepsilon \cos\Theta$. The rotation speeds of the shaft and the bearing shell are ω_i and ω_o, respectively. The origin of the xyz-coordinate system coincides with the center of the shell O_o and its z-axis has the same direction as the central axis of the bearing shell. The position of the shaft center O_i relative to the origin is described with the displacement $c\,\varepsilon$ and the angle δ (Cartesian displacements D_x and D_y).

The dynamical pressure build-up in the oil films of the bearing is described by the classic Reynolds fluid film equation, see e.g. [1, 8, 19]. In order to reduce the number of the coupling variables, the Reynolds equation is expressed in the dimensionless form used in [2],

$$\frac{\partial}{\partial\Theta}\left(H^3\frac{\partial\Pi}{\partial\Theta}\right) + \left(\frac{R}{B}\right)^2 \frac{\partial}{\partial z}\left(H^3\frac{\partial\Pi}{\partial z}\right) = \varepsilon(2\phi' - 1)\sin\Theta + 2\varepsilon'\cos\Theta\,. \tag{1}$$

The dimensionless pressure Π is defined by

$$\Pi = \left(\frac{c}{R}\right)^2 \frac{p}{6\eta(\omega_i + \omega_o)}\,, \tag{2}$$

where p represents the pressure and η the dynamic viscosity. The input variables of the bearing model are the eccentricity ε, the dimensionless squeeze speed ε' and the dimensionless whirl speed ϕ',

$$\varepsilon = \frac{1}{c}\sqrt{D_x^2 + D_y^2}\,, \qquad \varepsilon' = \frac{D_x\dot{D}_x + D_y\dot{D}_y}{c^2\varepsilon(\omega_i + \omega_o)}\,, \qquad \phi' = \frac{D_x\dot{D}_y - D_y\dot{D}_x}{c^2\varepsilon^2(\omega_i + \omega_o)}\,. \tag{3}$$

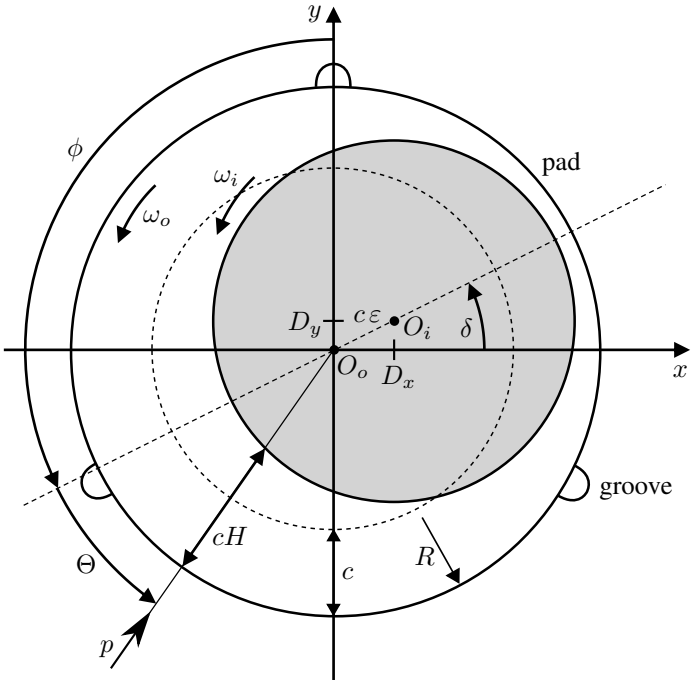

Figure 2: Geometry and kinematics of a cylindrical bearing with axial grooves.

In the Reynolds equation, only one parameter has to be specified, namely the ratio of the bearing radius R with respect to the bearing width B.

Equation (1) is discretized and solved with a commercial FEM tool. Modified boundary conditions for the axial grooves have to be taken into account in the inner oil film. The pressure at the boundaries of the grooves can be set to ambient pressure, because the depth of the grooves is much larger than the film thickness.

The resulting pressure field $p(\Theta, z)$ is integrated over the bearing shell which yields the forces in x and y-direction. For the inner oil film, the rotation of the axial grooves has to be taken into account.

The axial grooves also have an influence on the resulting bearing torque. The bearing torque acting on the shell is calculated by integration of the sheer stress

$$\tau_{xy} = R\eta \frac{\omega_i - \omega_o}{cH(\Theta)}\,, \tag{4}$$

over the surface of the bearing shell. Due to the grooves, equation (4) has to be integrated for each bearing pad separately. It should be pointed out that the resulting torque of a bearing with axial grooves is smaller compared to a plain cylindrical bearing.

2.3 Coupling Interface

The MBS and the FEM software are connected using a semi-implicit solver coupling approach, which is described in detail in ref. [3]. The coupled model and the information flow is schematically shown in Figure 3.

The rotor is modeled as a flexible multibody system, described by a system of DAEs of the form

$$\begin{aligned} \underline{\underline{M}}(\underline{q})\dot{\underline{u}} &= \underline{f}(\underline{q},\underline{u},t,\underline{u}^1_{\mathrm{MBS}},\ldots,\underline{u}^4_{\mathrm{MBS}}) - \underline{\underline{G}}^T(\underline{q},t)\underline{\lambda}\,, \qquad \dot{\underline{q}} = \underline{u} - \underline{\underline{G}}^T(\underline{q},t)\underline{\mu}\,, \\ \underline{0} &= \underline{g}(\underline{q},t)\,, \qquad\qquad\qquad\qquad \underline{0} = \underline{\underline{G}}^T(\underline{q},t)\underline{u} + \frac{\partial \underline{g}}{\partial t}(\underline{q},t)\,. \end{aligned} \tag{5}$$

The symmetric mass matrix is denoted by $\underline{\underline{M}}(\underline{q})$. The vectors of generalized coordinates and velocities are $\underline{q}$ and $\underline{u}$, respectively. The applied, gyroscopic and internal elastic forces are summarized in the vector $\underline{f}$. The vector $\underline{g}$ contains the algebraic constraint equations. The resulting constraint forces are $-\underline{\underline{G}}^T(\underline{q},t)\underline{\lambda}$ with the Jacobian $\underline{\underline{G}}(\underline{q},t) = \partial \underline{g}/\partial \underline{q}$ and the vector of Lagrange multipliers $\underline{\lambda}$. The correction term $-\underline{\underline{G}}^T(\underline{q},t)\underline{\mu}$ with the auxiliary Lagrange multipliers $\underline{\mu}$ is needed to fulfill constraints on position and velocity level simultaneously.

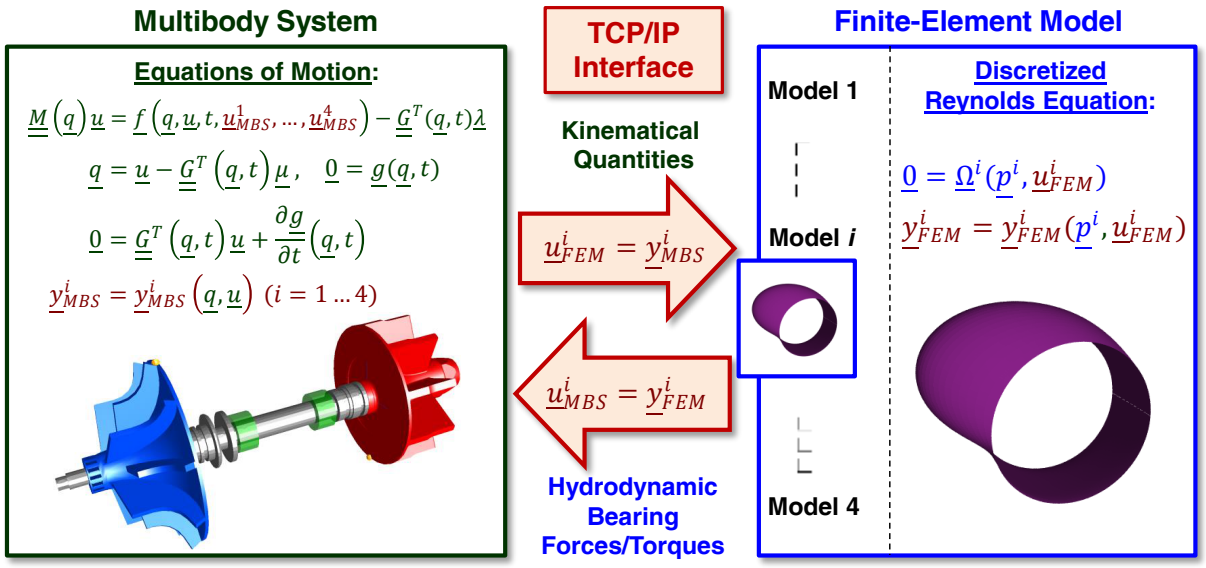

Figure 3: Force/displacement coupling approach between the turbocharger rotor and the bearing model [3].

The bearing forces are provided by the FEM software and are collected in the 4 MBS input vectors $\underline{u}^i_{\text{MBS}}$. The MBS output vectors $\underline{y}^i_{\text{MBS}}$ contain the kinematic quantities ε^i, ε'^i and ϕ'^i for each oil film, which are calculated from the displacements and the velocities collected in $\underline{q}$ and $\underline{u}$.

The bearings are represented by the discretized Reynolds equations. Discretization with a finite-element approach yields a set of algebraic equations $\underline{\Omega}^i$ for each oil film,

$$\underline{0} = \underline{\Omega}^i(\underline{p}^i, \underline{u}^i_{\text{FEM}}) \,. \tag{6}$$

The FEM system inputs are $\underline{u}^i_{\text{FEM}} = \underline{y}^i_{\text{MBS}}$. Solving (6) yields the pressure vector $\underline{p}$, which contains the pressure variables at the mesh nodes. Gümbel boundary conditions are used to account for cavitation effects. Integration of $\underline{p}$ gives the bearing forces, which are collected in the FEM output vector $\underline{y}^i_{\text{FEM}} = \underline{u}^i_{\text{MBS}}$.

Since only the rotor model is explicitly time-dependent, the MBS solver acts as master and calls the FEM solver. See ref. [3] for more details.

3 Simulation Results

Two dynamic run-up simulations with the described model are shown to investigate the influence of axial grooves in full-floating-ring bearings. In the first run-up simulation, a turbocharger with plain floating-rings – plain cylindrical bearing geometry in the inner and outer oil films – is used. Secondly, floating-rings with axial grooves in the inner fluid film are considered. The rotation speed of the turbine is increased linearly from 0 to 3500 Hz in 10 sec. The approximate simulation time was 30 days. Note that the width of the inner fluid film has been increased for the bearing with axial grooves, so that the total area of the inner bearing surface is equal for both bearing types.

Figure 4 shows the outer eccentricity of the compressor-sided ring for both bearing types. Only small differences between both simulations are observed up to a frequency of $\approx$1750 Hz. Then, the amplitude of the oscillation becomes larger for the turbocharger with axial grooves.

In Figure 5, inner eccentricities are shown. Here, the oscillation behavior is similar up to a frequency of $\approx$1200 Hz. The amplitudes of the turbocharger with axial grooves are smaller between $\approx$1200 Hz and $\approx$1400 Hz. The amplitudes then become larger for frequencies higher than $\approx$1800 Hz.

Figure 6 shows the waterfall diagram of the vertical oscillation of the measurement point at the compressor side for the turbocharger with plain cylindrical bearings. Besides the synchronous oscillation due to the imbalance excitation, we observe three subsynchronous oscillations. The first subsynchronous is generated by the oil whirl/whip of the inner oil film. The rotor oscillates in a conical forward mode. The second subsynchronous also results from the inner oil film, yet the rotor vibrates in a translational forward mode. The third subsynchronous is generated by the oil whirl/whip of the outer oil film. The rotor again oscillates in the conical forward mode. The

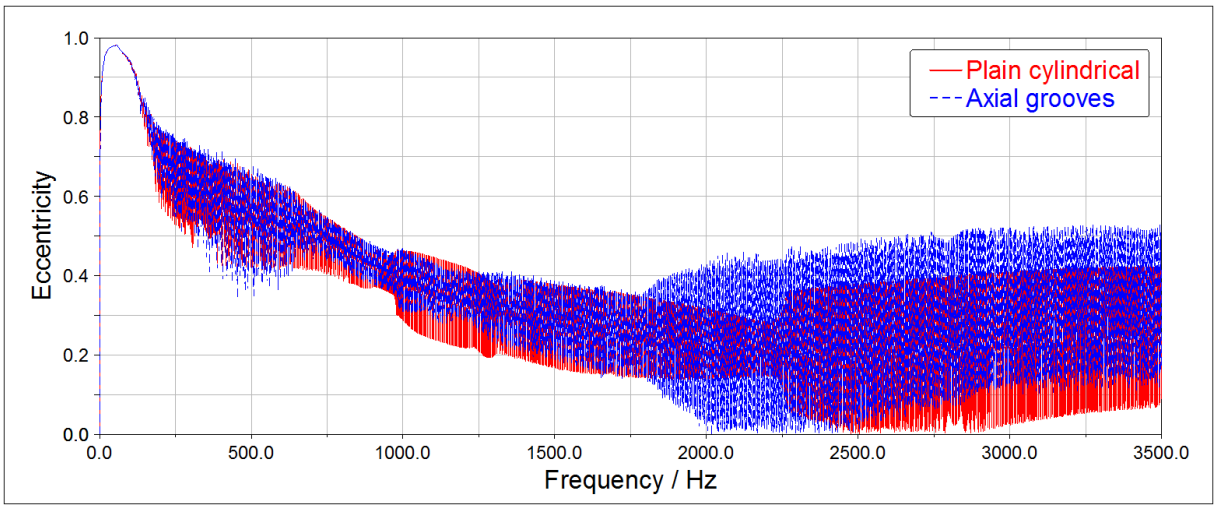

Figure 4: Outer eccentricity (floating-ring) in the bearing next to the compressor. Comparison between a turbocharger with plain cylindrical bearings (red) and a turbocharger with axial grooves in the inner surface of the floating-rings (blue).

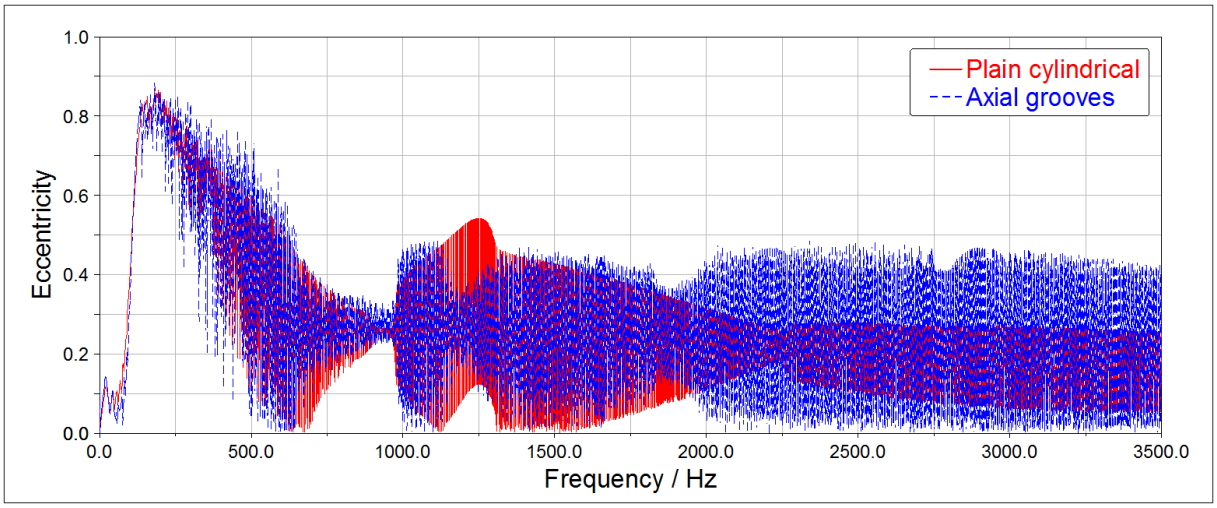

Figure 5: Inner eccentricity (rotor shaft) in the bearing next to the compressor. Comparison between a turbocharger with plain cylindrical bearings (red) and a turbocharger with axial grooves in the inner surface of the floating-rings (blue).

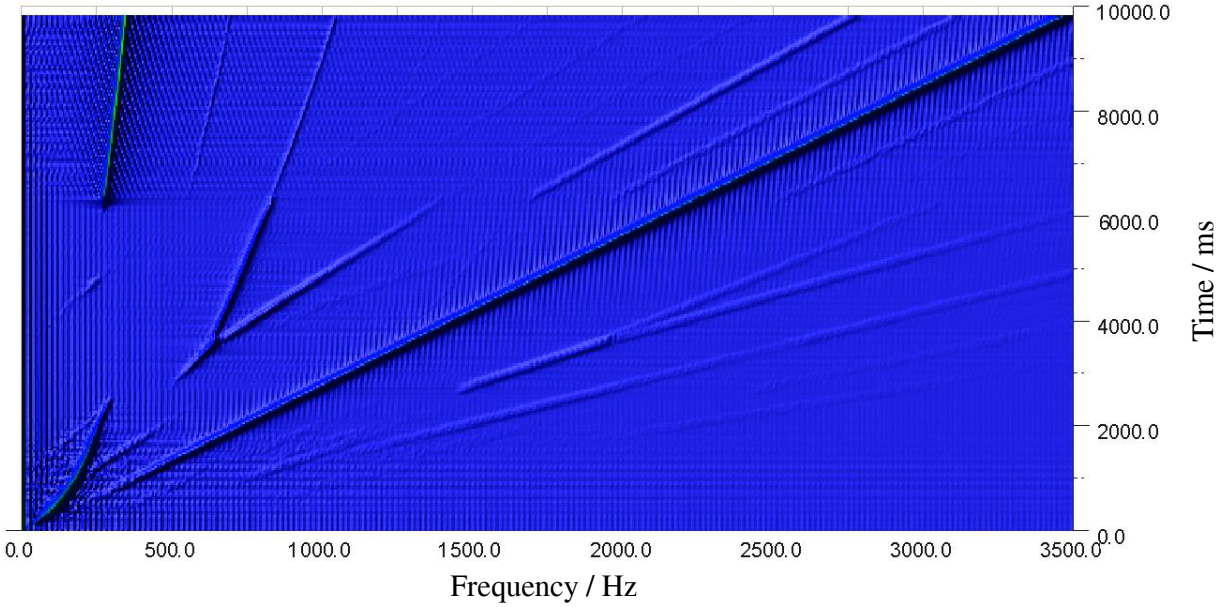

Figure 6: Waterfall diagram of the vertical oscillation of the measurement point at the compressor side. Turbocharger with plain cylindrical bearings.

1st subsynchronous oscillation is visible up to ≈ 850 Hz. The 2nd subsynchronous oscillation can be seen between ≈ 950 Hz and ≈ 1300 Hz. The onset of the 3rd subsynchronous oscillation is at ≈ 2200 Hz.

Figure 7 shows the waterfall diagram for the turbocharger with axial grooves. Again, three subsynchronous oscillations can be observed. The 1st subsynchronous – similar to the case with plain bearings – can be seen up to ≈ 750 Hz. However, the 1st subsynchronous vanishes at a lower frequency compared to the simulation with plain bearings. The 2nd subsynchronous oscillation becomes distinctively smaller and ranges now from ≈ 1000 Hz to ≈ 1100 Hz. The onset of the 3rd subsynchronous oscillation occurs at ≈ 1750 Hz, at a much lower frequency compared to the turbocharger with plain bearings.

4 Conclusion

The influence of axial grooves in full-floating-ring bearings on the oscillation behavior of turbochargers has been investigated numerically. A coupled model was used, consisting of a rotor and a bearing model. The rotor was

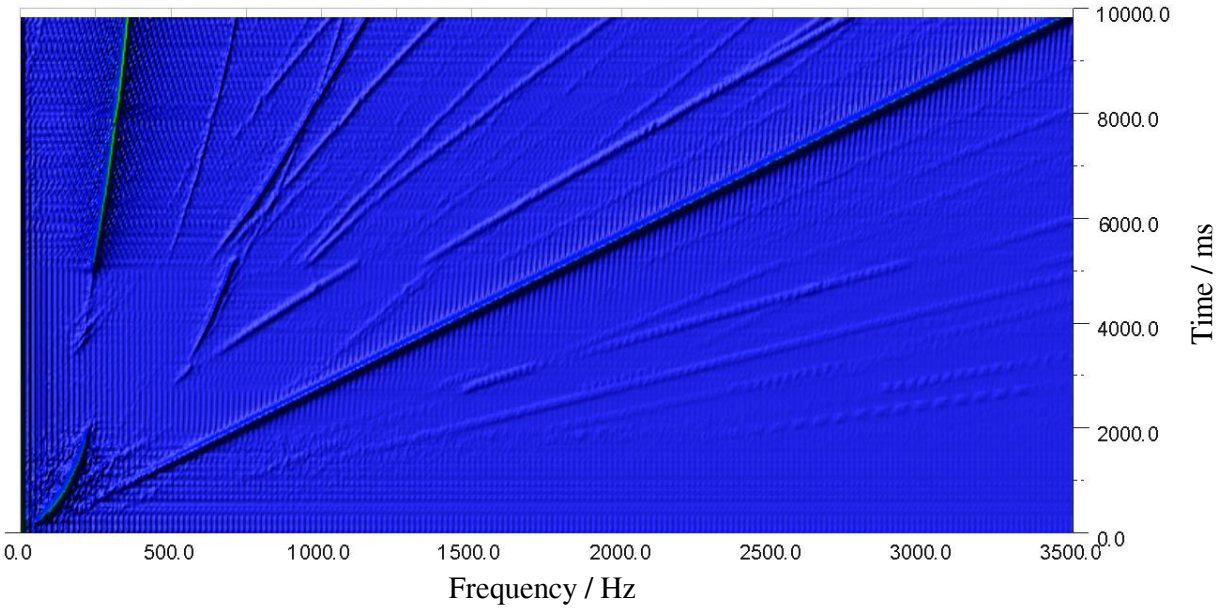

Figure 7: Waterfall diagram of the vertical oscillation of the measurement point at the compressor side. Turbocharger with axial grooves in the inner surface of the floating-rings.

modeled in a commercial MBS software. The Reynolds fluid film equation was discretized using a commercial FEM software. In contrast to approximate solutions – such as the short-bearing solution – bearing geometries can be investigated that are more complex and a physically better solution is achieved with the cost of longer computation times.

The results of a run-up simulation with axial grooves in the inner surface of the floating-rings were compared to a run-up simulation using plain cylindrical bearings. It was observed that the amplitude of the 2nd synchronous oscillation can be reduced with axial grooves. On the contrary, the onset of the 3rd synchronous is shifted to a lower frequency and the amplitude is significantly increased.

REFERENCES

[1] Bartel, D. (2010): *Simulation von Tribosystemen: Grundlagen und Anwendungen*. Vieweg+Teubner research. Vieweg Verlag, Friedrich & Sohn Verlagsgesellschaft mbH.

[2] Boyaci, A. (2011): *Zum Stabilitäts- und Bifurkationsverhalten hochtouriger Rotoren in Gleitlagern*. Ph.D. Dissertation, Karlsruher Institut für Technologie, Karlsruhe.

[3] Busch, M., Schweizer, B. (2011): Coupled simulation of multibody and finite element systems: an efficient and robust semi-implicit coupling approach. *Arch. Appl. Mech.*, **82**, pp. 723–741.

[4] Daniel, C., Nitzschke, S., Woschke, E., Strackeljan, J. (2013): Identifikation des Einfluss konstruktiver Lagerparameter eines in Schwimmbuchsen gelagerten Rotorsystems. In *SIRM, 10. Internationale Tagung Schwingungen in rotierenden Maschinen*. Berlin, Germany, Feb. 25-27.

[5] Flack, R.D., Lanes, R.F. (1982): Effects of three-lobe bearing geometries on rigid-rotor stability. *ASLE Trans.*, **25(2)**, pp. 221–228.

[6] Flack, R.D., Kostrzewsky, G.J., Barrett, L.E. (2002): Experimental and Predicted Rigid Rotor Stability Threshold of Axial Groove and Three-Lobe Bearings. *Int. J. of Rotating Machinery*, **8(1)**, pp. 27–33.

[7] Kirk, R.G. (2013): Experimental Evaluation of Hydrodynamic Bearings for a High Speed Turbocharger. In *Proc. of ASME Turbo Expo 2013*. San Antonio, Texas, USA, June 3-7, pp. 1–9.

[8] Khonsari, M.M., Booser, E.R. (2008): *Applied Tribology: Bearing Design and Lubrication*. Tribology in Practice Series. Wiley.

[9] Köhl, W., Kreschel, M. (2014): Experimental and numerical investigations on an automotive turbocharger with a transparent bearing section. In *IMechE, 11th Int. Conf. on Turbochargers and Turbocharging*. London, UK, May 13-14, pp. 349–359.

[10] Lanes, R.F., Flack, R.D. (1982): Effects of Three Lobe Bearing Geometries on Flexible Rotor Stability. *ASLE Trans.*, **25(3)**, pp. 377–385.

[11] Lanes, R.F., Flack, R.D., Lewis, D.W. (1982): Experiments on the Stability and Response of a Flexible Rotor in Three Types of Journal Bearings. *ASLE Trans.*, **25(3)**, pp. 289–298.

[12] Li, D.F., Choy, K.C., Allaire, P.E. (1980): Stability and Transient Characteristics of Four Multilobc Journal Bearing Configurations. *ASME Journal of Lubrication Technology*, **102(3)**, pp. 291–299.

[13] Nitzschke, S.; Woschke, E.; Daniel, C. und Strackeljan, J. (2011): Simulation von Schwimmbuchsenlagerungen in Abgasturboladern. *Journal of Mechanical Engineering of the National Technical University of Ukraine KPI, Kiew*.

[14] Nguyen-Schäfer, H. (2013): Nonlinear Rotordynamic Computations of Automotive Turbochargers Using Rotating Floating Ring Bearings at High Rotor Speeds. In *SIRM, 10. Internationale Tagung Schwingungen in rotierenden Maschinen*. Berlin, Germany, Feb. 25-27.

[15] Nguyen-Schäfer, H. (2012): *Rotordynamics of Automotive Turbochargers.*. Springer Heidelberg New York Dordrecht London.

[16] Schweizer, B., Sievert, M. (2009): Nonlinear oscillations of automotive turbocharger turbines. *Journal of Sound and Vibration*, **321**, pp. 955–975.

[17] Schweizer, B. (2009): Total instability of turbocharger rotors – Physical explanation of the dynamic failure of rotors with full-floating-ring bearings. *Journal of Sound and Vibration*, **328**, pp. 156–190.

[18] Schweizer, B. (2010): Dynamics and stability of turbocharger rotors. *Arch. Appl. Mech.*, **80**, pp. 1017–1043.

[19] Szeri, A.Z. (2011): *Fluid Film Lubrication*. Cambridge University Press.

[20] Tomm, U., Boyaci, A., Proppe, C., Seemann, W., Esmaeil, L., Schweizer, B. (2009): Rotor dynamic analysis of a passenger car turbocharger using run-up simulation and bifurcation theory. In *IMechE, 9th Int. Conf. on Turbochargers and Turbocharging*. London, UK, May 19-20, pp. 335–347.